A New Phasor Estimator for PMU Applications: P Class and M Class

Jose R. Razo-Hernandez, Arturo Mejia-Barron, David Granados-Lieberman, Martin Valtierra-Rodriguez, and Jose F. Gomez-Aguilar

***Abstract*—Phasor measurement units (PMUs) are fundamental tools in the applications of modern power systems, where synchronized phasor estimations are needed. The accuracy and dynamic performance requirements for phasor, frequency, and rate of change of frequency (ROCOF) estimations are established in the IEEE Std. C37.118.1-2011 along with the IEEE Std. C37.118.1a-2014, where two PMU performances are suggested: P class filters for applications requiring fast response and M class filters for applications requiring high rejection to aliased signals. In this paper, a methodology to design new phasor estimators that satisfy the P class and M class requirements in PMUs is presented. The proposed methodology is based on finite impulse response filters, brick-wall filters, and complex filter design concepts, where frequency range, time performance, harmonic rejection and out-of-band interference requirements are considered in its design. A comparative analysis using the reference model given by the IEEE Std. C37.118.1 is presented. The results show the effectiveness of the phasor estimators under steady-state and dynamic conditions according to the PMU standard, making them suitable tools for applications in power systems.**

***Index Terms*—Brick-wall filter, complex filter, IEEE Std. C37.118.1, M class, P class, phasor measurement unit (PMU), phasor estimator.**

I. Introduction

PHASOR measurement units (PMUs) have become powerful and reliable tools for many power grid applications as stand-alone units or in conjunction with other units, allowing to visualize the condition of a whole power system [1]-[3] and providing important information for many applications in modern power systems. The PMU requirements for synchronized phasor, frequency, and rate of change of frequency (ROCOF) measurements are defined in the IEEE Std. C37.118.1 [4], [5]. According to this standard, there are two classes of performance: P class and M class, implying different requirements and processing models. P class is intended for applications that require fast response, whereas M class is preferred for applications that require a high rejection to aliased signals [4], i.e., a greater precision. Although the IEEE Std. C37.118.1 presents a heterodyne process along with a triangular weighted finite impulse response (FIR) filter for P class or a brick-wall low-pass FIR filter for M class, this standard does not restrict the method used to compute the abovementioned parameters. Therefore, many phasor estimators have been proposed in the scientific literature.

The discrete Fourier transform (DFT) has been widely used as phasor estimator due to its simplicity; regrettably, its poor performance under dynamic conditions [6], [7] compromises the compliance with the standard, leading to the development of new DFT-based algorithms. The interpolated DFT (IpDFT) has been tested for P class and M class PMUs [8], [9]. Although the most standard requirements are satisfied, the out-of-band (OOB) interference test, which is a benchmark test for M class PMUs, is still a difficult issue to solve. Additionally, different techniques such as the Taylor series [10], wavelet transform [11], recursive least-squares [12], and Kalman filter among others [1], [13] have also been proposed to provide solutions that improve the performance presented in traditional DTF-based techniques under dynamic conditions. However, there is no evidence that these techniques can satisfy all the requirements stated in the standard for P class and M class. In [14], a dynamic phasor model based on the Taylor series that satisfies all the requirements for M class PMUs including the OOB test, is presented. However, in order to satisfy this test, an additional filtering stage is proposed. Although promising results are obtained, this filter represents both an extra delay time and additional computation resources. In [15], the Hilbert transformation and the convolution technique are proposed for phasor estimation in P class PMUs, where the compliance tests stated in [5] are fulfilled. It should be pointed out that the magnitude estimation using the Hilbert transformation can be negatively affected when the analyzed signal is not a monocomponent signal, e. g., a signal with interharmonic components. In this regard, the implementation of the Hilbert transformation in M class PMUs can be an unsuitable

Manuscript received: September 4, 2018; accepted: June 19, 2019. Date of CrossCheck: June 19, 2019. Date of online publication: November 26, 2019.

J. R. Razo-Hernandez, A. Mejia-Barron, and M. Valtierra-Rodriguez (corresponding author) are with the ENAP-Research Group, Facultad de Ingeniería, Universidad Autónoma de Querétaro (UAQ), San Cayetano, C. P. 76807, México (e-mail: roberto.razo@enap-rg.org; arturo.mejia@enap-rg.org; martin.valtierra@enap-rg.org).

D. Granados-Lieberman is with the ENAP-Research Group, Departamento de Ingeniería Electromecánica, Instituto Tecnológico Superior de Irapuato (ITESI), Colonia El Copal, C.P. 36821, México (e-mail: david.granados@enap-rg.org).

J. F. Gomez-Aguilar is with the CONACyT-Centro Nacional de Investigación y Desarrollo Tecnológico (CENIDET), Tecnológico Nacional de México, Interior Internado Palmira S/N, Col. Palmira, C. P. 62490, México (e-mail: jgomez@cenidet.edu.mx).

DOI: 10.35833/MPCE.2018.000584

choice if a poor filtering stage is applied to extract the fundamental component.

In order to simplify the implementation of the phasor estimator for each class and the PMU setup for different applications in power systems, some works have presented several techniques and methodologies to satisfy both P class and M class PMU requirements for a single methodology [16]-[19]. However, the accomplishment of all the requirements for P class and M class through the same algorithm is a very difficult task, mainly considering the dynamic and steady-state evaluations of parameters such as total vector error (TVE), frequency error (FE), and ROCOF error (RFE) [4], [5]. In [16], the generalized Taylor weighted least square-IpDFT (GTWLS-IpDFT) is presented, complying with all the requirements for P class and M class. However, a proper number of the waveform cycles have to be considered and the most significant disturbances have to be removed from the analyzed signal. In [17], an algorithm to satisfy both P class and M class of PMUs is presented which is called iterative-IpDFT (i-IpDFT). Although the algorithm satisfies the requirements stated in the IEEE Std. C37.118.1, the iterative procedure requires a convergence time in the function of the number of iterations, where the accuracy increases according to this number. In [18], two algorithms, namely P class asymmetric algorithm and M class TickTock algorithm, using adaptive cascaded filters have been presented. As abovementioned, adaptive techniques present some issues that have to be considered in continuous monitoring applications. In [19], a PMU scheme based on the Taylor-Fourier transform (TFT) is proposed, where two channels using two different TFT configurations, i.e., two different orders. And a detector is presented for P class and M class requirements, which chooses the proper output from the two channels according to the properties of the input signals in steady state or with fast changes. Although promising results are obtained in [20],[21], the fulfilment of the OOB test is still an unsolved issue.

In this paper, the new phasor estimators based only on filters for P class and M class PMUs are proposed. The designed filters are complex brick-wall band-pass FIR filters which are used to generate the analytic signal of the fundamental component. With the analytic signal, the phasor estimation (magnitude, phase, and frequency for the fundamental component) is carried out [4]. Once the filters are designed, no additional processing steps during the phasor estimation are required unlike other works that implement several algorithms in a continuous way, reducing both the complexity and the computational burden. It should be pointed out that simple filters cannot satisfy the specifications stated in [4], [5]. Therefore, a filter design methodology which takes into account different requirements of each PMU class such as low computation burden, fast response, high accuracy, and high rejection to both harmonic and inter-harmonic components is proposed as the main contribution. The obtained filters differ only in size for each class, simplifying their implementation and the PMU setup for different applications in power systems. In general, the design considers a band-pass filter constructed from two brick-wall low-pass filters, which is the real part in a complex filter context. Then, the frequency response of the real filter is set in quadrature along with a weighting function to construct the imaginary filter through the weighted least square (WLS) algorithm. The proposed weighting function allows getting both a great fitting in the magnitude frequency response of the imaginary filter in the PMU frequency range and a high rejection to harmonic components. The obtained filters are put into a PMU scheme and validated using all the tests stated in the IEEE Std. C37.118.1-2011 and Std. C37.118.1-2014. A comparative analysis using the standard reference algorithms is presented. The results show that the proposal can fully satisfy all the requirements under static and dynamic conditions, including the OOB test which is one of the most difficult tests.

II. Theoretical Background

A. IEEE Std. C37.118.1

The IEEE Std. C37.118.1 presents two classes of PMUs: P class and M class. The algorithm presented in the standard for phasor estimation corresponds to a heterodyne process where the demodulation is carried out by low-pass filters. For P class, a two-cycle triangular weighted FIR filter with fixed length is presented, which is good enough for applications that need a fast response time. On the other hand, a requirement for the M class is the attenuation of the signals above the Nyquist frequency for the given reporting rate by at least 50 dB. In this regard, the standard presents a brick-wall filter due to its ideally flat amplitude response and great attenuation for harmonics and inter-harmonics. To establish the effectiveness of the phasor estimator, the standard presents different static and dynamic tests, where the most important parameters used to evaluate its compliance are TVE, FE, and RFE. The TVE is a quantity to evaluate the total vector error that exists between an ideal phasor value (theoretical value) and a measured phasor value. It is defined by [4]:

$$TVE(n)=\sqrt{\frac{\left(X_r'(n)-X_r(n)\right)^2+\left(X_i'(n)-X_i(n)\right)^2}{\left(X_r(n)\right)^2+\left(X_i(n)\right)^2}} \tag{1}$$

where $X_r'(n)$ and $X_i'(n)$ are the measured values; $X_r(n)$ and $X_i(n)$ are the theoretical values; n is the current sample in discrete time; the subscript "r" stands for the real part of a complex number; and the subscript "i" stands for the imaginary part of a complex number. The FE is defined as the absolute difference between the theoretical frequency $f(n)$ and the estimated frequency $f'(n)$ as follows:

$$FE=\left|f(n)-f'(n)\right| \tag{2}$$

The RFE is defined as the absolute difference between the derivative of the frequency theoretical value $\mathrm{d}f(n)/\mathrm{d}t$, and the estimation of the derivative of the measured frequency $\mathrm{d}f'(n)/\mathrm{d}t$. It is measured in Hz/s and given by:

$$RFE=\left|\frac{\mathrm{d}f(n)}{\mathrm{d}t}-\frac{\mathrm{d}f'(n)}{\mathrm{d}t}\right| \tag{3}$$

The limit values for TVE, FE and RFE are established by

the IEEE Std. C37.118.1-2011 [4] and the updates in the IEEE Std. C37.118.1a-2014 [5] by considering static tests, dynamic tests and step change tests.

B. Conceptualization of Complex Brick-wall Band-pass Filter

Linear phase FIR filters are commonly used due to their stability and immunity to the phase distortion [21]. In this sense, a brick-wall filter is considered as an idealized filter with a rectangular frequency response and an abrupt transition between the passband and the stopband [22]. The impulse response for a low-pass filter h_{LP} is given by a sinc function as follows:

$$h_{LP}(k)=\operatorname{sinc}\left(2\pi\times 2F_{fr}/F_{samp}\,k\right)=\frac{\sin\left(2\pi\times 2F_{fr}/F_{samp}\,k\right)}{2\pi\times 2F_{fr}/F_{samp}\,k} \quad (4)$$

where F_{fr} is the reference frequency for the low-pass brick-wall filter; k is the k^{th} filter coefficient; F_{samp} is the sampling frequency; and $h_{LP}(0)=1$. In addition, this low-pass filter can be multiplied by a Hanning function $H_{hann}(k)$ in order to reduce the ripple in its frequency response. The filter coefficients can be normalized at 0 Hz by dividing them by their summation:

$$h'_{LP}(k)=h_{LP}(k)H_{hann}(k)/G_{filter} \quad (5)$$

where G_{filter} is the gain of the filter and set to be 0 Hz.

The band-pass filter coefficient h_{BP} can be achieved as the difference of two low-pass filters and each filter is designed by (5). The first low-pass filter has a cutoff frequency given by the lower band edge h'_{LP_L}, and the second filter has a cutoff frequency given by the upper band edge h'_{LP_U}. The resulting filter coefficients are defined as:

$$h_{BP}(k)=h'_{LP\_U}(k)-h'_{LP\_L}(k) \quad (6)$$

On the other hand, the complex FIR filters can be expressed as:

$$h(k)=h_{cos}(k)+\mathrm{j}h_{sin}(k) \quad (7)$$

where $h_{cos}(k)$ and $h_{sin}(k)$ are the normalized coefficients corresponding to the real and imaginary coefficients of the complex filter, respectively. In this paper, each part corresponds to a brick-wall band-pass filter given in (6). As a result, the components in quadrature (analytic signal) of the input signal are obtained.

In a complex filter, the imaginary filter could be obtained using FFT [23], [24]. However, the number of coefficients compromises the frequency resolution. Therefore, the imaginary coefficient h_{sin} is computed using the real coefficient h_{cos}. If the frequency response for the imaginary part is assumed as a frequency response in quadrature of the real part $H_{cos}(\mathrm{j}\omega)$, the expected frequency response for the imaginary part $H_{sin}(\mathrm{j}\omega)$ is computed as the rotation of $H_{cos}(\mathrm{j}\omega)$ by $-\pi/2$ ($-90°$) as follows:

$$H_{sin}(\mathrm{j}\omega)=-\mathrm{j}H_{cos}(\mathrm{j}\omega) \quad (8)$$

Once the frequency response $H_{sin}(\mathrm{j}\omega)$ is obtained, the coefficient of the imaginary part $h_{sin}(k)$ can be computed using a WLS algorithm, where the main idea is to fit the coefficients into a FIR filter transfer function $D(z)$ with the same order of H_{cos} [25] as follows:

$$D(z)=\sum_{k=-K/2}^{K/2}a(k)z^{-k} \quad (9)$$

where K is the filter order; and $a(k)$ is the filter coefficient. Then, the frequency response data $H_{sin}(\mathrm{j}\omega)$ is used to estimate the transfer function by minimizing a cost function J given by [26]:

$$J=\sum_{m=1}^{F}W(\mathrm{j}\omega_m)\left|H_{sin}(\mathrm{j}\omega_m)-D(\mathrm{j}\omega_m)\right|^2 \quad (10)$$

where $W(\mathrm{j}\omega_m)$ is a weighting cost function used to improve the fit in specific frequency ranges; and m is the frequency component. This function is evaluated up to the Nyquist frequency, i.e., $F=F_{samp}/2$. It should be pointed out that the selection of the $W(\mathrm{j}\omega_m)$ values depends on the user experience since there are not specific rules for each application [26].

III. Proposed Methodology

The proposed PMU implementation is mainly divided into 3 stages as shown in Fig. 1.

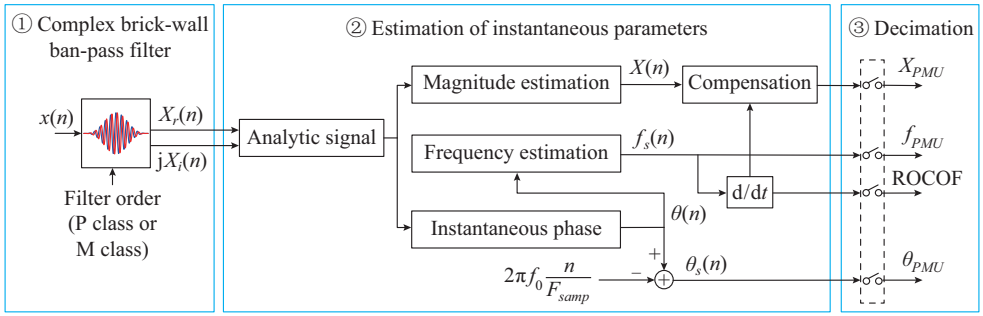

Fig. 1. Proposed PMU including P class and M class.

They are: ① the design methodology for the complex brick-wall band-pass filter (main contribution); ② the estimation of the instantaneous parameters (magnitude, phase, frequency, and ROCOF); ③ the decimation.

In the first stage, the phasor estimation is carried out by considering a dynamic fundamental signal expressed as [14]:

$$x(n)=X(n)\cos\left(\sum_{n=0}^{N-1}2\pi f(n)/F_{samp}+\phi_0\right)=X(n)\cos\left(2\pi f_0 n/F_{samp}+\sum_{n=0}^{N-1}2\pi\Delta f(n)/F_{samp}+\phi_0\right) \quad (11)$$

where $X(n)$ is the instantaneous amplitude of the signal; $f(n)$

is the signal frequency with initial phase ϕ_0; f_0 is the nominal frequency; $\Delta f(n)$ is the instantaneous frequency deviation; and N is the length of the signal.

In a complex reference frame, (11) is represented by:

$$x(n)=X(n)\mathrm{e}^{\mathrm{j}\theta(n)}=X_r(n)+\mathrm{j}X_i(n) \tag{12}$$

where $\theta(n)$ is the instantaneous phase which is given by:

$$\theta(n)=2\pi f_0 n/F_{samp}+2\pi\sum_{n=0}^{N-1}\Delta f(n)/F_{samp}+\phi_0 \tag{13}$$

From (12), the instantaneous magnitude can be computed as:

$$X(n)=\frac{1}{\sqrt{2}}\sqrt{X_r^2(n)+X_i^2(n)}\Big/Gain \tag{14}$$

where $Gain$ is the compensation factor given by $Gain=\sum_{k=0}^{N-1}h(k)\mathrm{e}^{-\mathrm{j}wk}$ and w is the estimated frequency. Therefore, its value varies in function of the instantaneous frequency deviation $\Delta f(n)$. This compensation is required because the frequency deviation affects the filter performance according to its frequency response, and therefore the magnitude estimation. In a similar way, the instantaneous phase can be computed from (12). The phase angle between the two signals in quadrature $X_r(n)$ and $X_i(n)$ is:

$$\theta(n)=\arctan\left(X_i(n)/X_r(n)\right) \tag{15}$$

It is important to mention that this phase corresponds to the argument of the sinusoidal function in (11). In this regard, the phase is measured in a rotating reference frame with an angular frequency of $2\pi f_0$. For syncrophasors, it is usual to remove the first term of (13) in order to obtain an instantaneous phase $\theta_s(n)$ in a stationary reference frame [4], [14]. In this case, it is estimated as:

$$\theta_s(n)=\theta(n)-2\pi f_0 n/F_{samp} \tag{16}$$

The instantaneous frequency is estimated by deriving the instantaneous phase $\theta(n)$, which is carried out by a third-order FIR filter structure, with coefficient $b_k=\{12,-6,-4,-2\}/(20/F_{samp})$. This derivative filter is based on the frequency estimation algorithm presented in [4]. Then, the instantaneous frequency is obtained as [4]:

$$f_s(t)=\frac{1}{2\pi}\frac{\mathrm{d}\theta}{\mathrm{d}t} \tag{17}$$

From $f_s(t)$, the ROCOF is computed by [4]:

$$ROCOF(t)=\frac{\mathrm{d}f_s(t)}{\mathrm{d}t} \tag{18}$$

In the last stage, the decimation of the instantaneous values is performed at the desired reporting rate F_s = 60 fps, in order to obtain the results X_{PMU}, θ_{PMU}, f_{PMU} and ROCOF.

For the design of complex filters (those used in the first stage), the proposed methodology is depicted in Fig. 2, which is applied for both P class and M class.

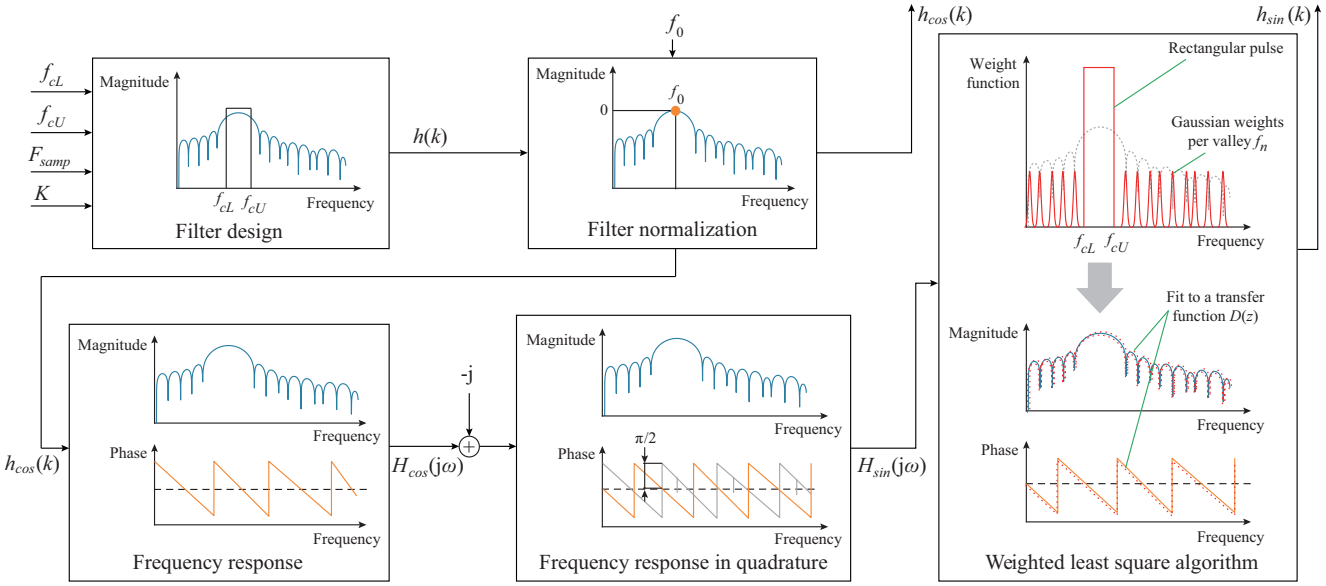

Fig. 2. Proposed methodology for complex FIR filter design.

Firstly, the brick-wall band-pass filter coefficient $h(k)$ is obtained using (4)-(6). The range from reference frequency f_{cL} to f_{cU} is 29-31 Hz for P class and 27.5-32.5 Hz for M class, where f_{cL} is the cutoff frequency given by the lower band edge and f_{cU} is the cutoff frequency given by the upper band edge. The sampling frequency F_{samp} is 6000 samples per second and the filter order is set up at 200 for P class and 900 for M class, respectively. These orders represent the filters of 2 and 9 cycles, respectively, which are similar to those used by the IEEE Std. C37.118.1. The real band-pass filter is normalized at the nominal frequency f_0 = 60 Hz, to obtain a unit gain in the magnitude at f_0. This process is carried out by dividing the filter coefficient $h(k)$ by the magnitude of the filter frequency response $|H(\mathrm{j}\omega)|$ at f_0 as follows:

$$h_{cos}(k)=h(k)/\left|H(\mathrm{j}2\pi f_0)\right| \tag{19}$$

As abovementioned, a rotation of the frequency response $h_{cos}(k)$ is carried out by (8), generating the same magnitude frequency response but with a phase shift of $-\pi/2$. Then, the rotated frequency response $H_{sin}(\mathrm{j}\omega)$ is fitted to a Kth order

FIR filter architecture defined by (9) through the minimization of the cost function given by (10). The proposed weighting function is tuned into the bandwidth of each filter as a rectangular pulse function with a magnitude of 1.0×10^{9}, which is set heuristically to obtain the same magnitude behavior for the real and imaginary parts of the complex filter in the passband region. With this, a huge weight or importance is given to the passband region during the fit whereas the other regions are not so important. This range encompasses the area of interest for the PMU application, i.e., F_{cL} to F_{cU}. Additionally, a train of Gaussian functions f_n is proposed at each valley of the side lobes according to the magnitude filter frequency response. These weights are proposed to have a good fit along all the filter frequency responses, allowing good rejection to harmonic content in the stop band. The Gaussian function is defined by:

$$f_{HN} = \sum_{f=0}^{F} M_g \mathrm{e}^{-\left(\frac{f-f_n}{2}\right)^2} \tag{20}$$

where M_g is a constant of 1×10^{5}; F is the maximum number of frequencies; and f_n corresponds to the frequency of each valley of the side lobes. These values must be estimated for each filter class. The rest of the weights are unitary. In a similar way, a big value of M_g is chosen in order to obtain a great fit in the side lobes. Figure 3(a) shows the magnitude filter frequency response for P class along with a zoomed area, where $H_{cos}(\mathrm{j}\omega)$ and $H_{sin}(\mathrm{j}\omega)$ have a great fit at the fundamental component and a magnitude response with an attenuation over 50 dB for the second harmonic. Besides, the desired phase shift of $-\pi/2$ is achieved into the filter bandwidth. Therefore, although a low order is proposed for this filter (K = 200), the requirements of high harmonic rejection and low latency for P class are fulfilled. On the other hand, a more abrupt response around the bandwidth is obtained when the filter order is K = 900 shown in Fig. 3(b), improving the harmonic and OOB interference rejection. In fact, an attenuation greater than 50 dB is obtained for frequencies beyond the Nyquist frequency (30 Hz). These features are suitable for M class PMUs. Although the latency increases for M class due to the filter order, it does not exceed the allowable limits. Finally, the coefficients $h_{cos}(k)$ and $h_{sin}(k)$ for the proposed complex filters are obtained.

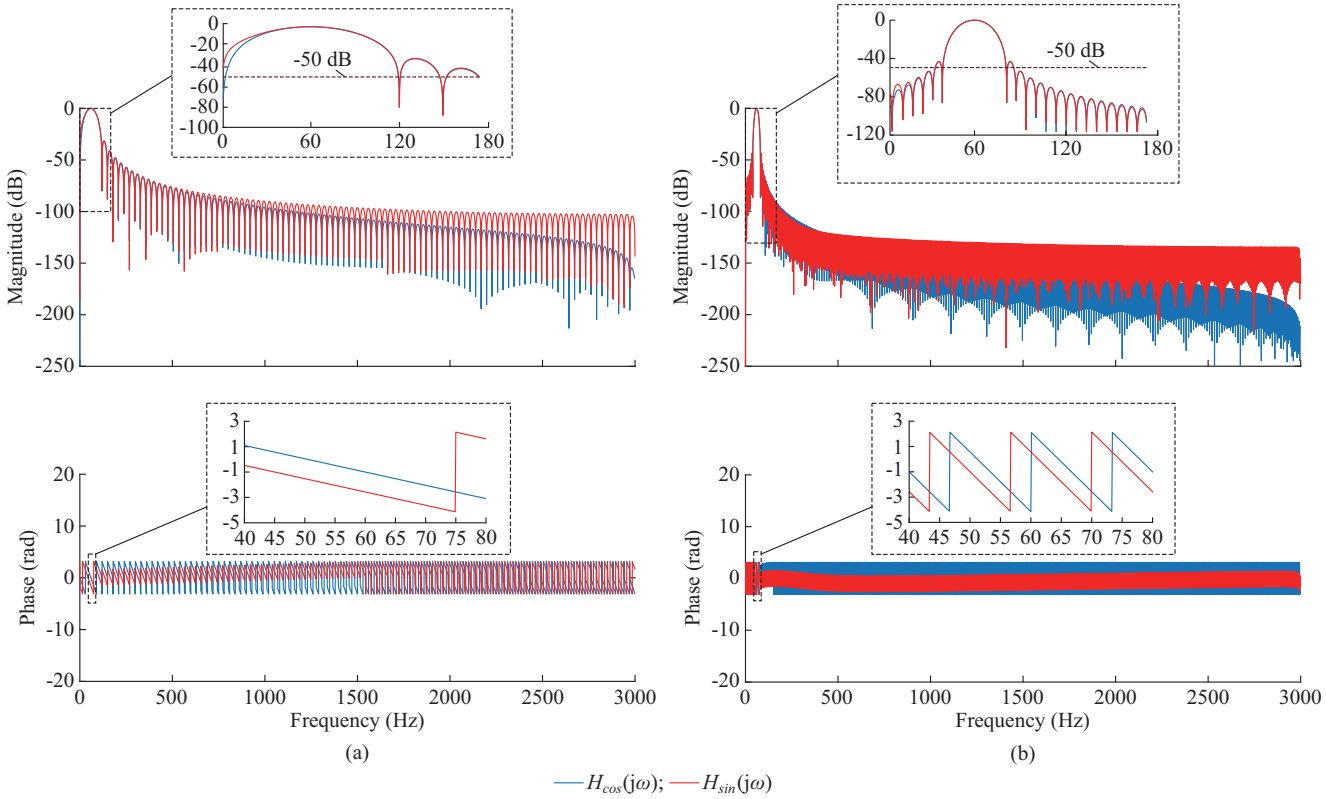

Fig. 3. FIR filter frequency response. (a) P class. (b) M class.

IV. Experimentation and Results

In this section, the results obtained by the proposed algorithm are presented. For comparison purposes, the results obtained by the reference model from the IEEE Std. C37.118.1 are also shown. Since both algorithms, i.e., the proposal and the reference model, are based exclusively on filters and require neither frequency-tracking algorithms nor other processing stages, a fairer comparison can be carried out.

A. Steady-state Test

1) Magnitude Test

The magnitude test is carried out by evaluating the amplitude of a synthetic sinusoidal signal that ranges from 0.8 to 1.2 p.u. for voltage applications and from 0.1 to 2 p.u. for current applications. The allowable accuracy for phasor estimation is limited to a TVE value of 1%. As shown in Fig. 4(a) and (b), the obtained TVE values for each condition are far below 1% for P class and M class.

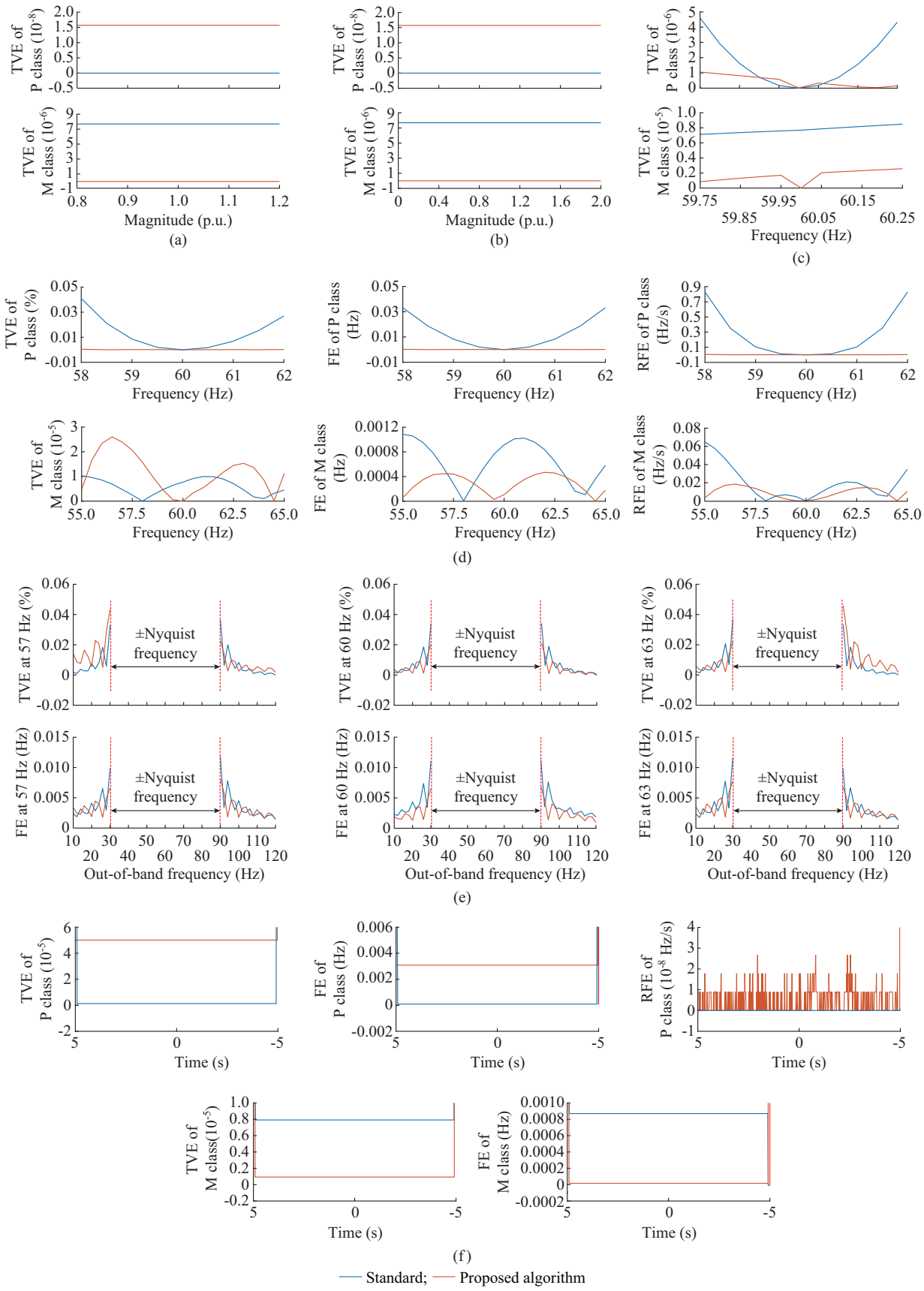

Fig. 4. Static tests for a PMU: P class and M class. (a) Voltage magnitude test. (b) Current magnitude test. (c) Phase test. (d) Frequency test. (e) OOB test only for M class. (f) THD test.

Likewise, maximum error values are listed in Table I in order to compare the accuracy for both algorithms (the proposed algorithm and the one presented by the IEEE Std. C37.118.1) where lower TVE values are reached in the standarad algorithm for P class with a TVE error of 2.34×10^{-14} against 1.57×10^{-8} of the proposed algorithm. However, a lower error is achieved by the proposed algorithm for M class with a TVE of 9.93×10^{-10}. In general, both algorithms provide accurate results by considering that the TVE limit is 1%.

2) Phase Test

In this test, phase conditions within $\pm\pi$ rad are achieved by means of frequency deviations from 59.75 to 60.25 Hz as described in [4] for both P class and M class. As shown in Fig. 4(c), the phasor accuracy is evaluated by the TVE values where both algorithms are within the required accuracy. Likewise, the maximum TVE values are listed in Table I, where TVE values of 4.60×10^{-6} and 8.49×10^{-6} are respectively obtained for P class and M class using the reference model algorithm, while for the proposed algorithm, lower errors are obtained, i.e., 1.05×10^{-6} and 2.57×10^{-6}, respectively.

3) Frequency Test

The frequency test is used to assess phasor and frequency estimation with frequency deviations by means of a synthetic signal with the changes in the fundamental frequency that ranges from 58 to 62 Hz for P class and from 55 to 65 Hz for M class. The phasor estimation accuracy is within allowable limits for the reference model and the proposed algorithm as shown in Fig. 4(d). Regrettably, some drawbacks for frequency and ROCOF estimations appear in the IEEE reference model when the frequency is farther from the nominal value, reaching inadmissible accuracy values for P class in the frequency and ROCOF estimations. The obtained values are 0.0331 Hz and 0.8291 Hz/s for FE and RFE, respectively, as shown in Table I. This is associated to the low rejection to the harmonic and interharmonic components of the triangular filter proposed by the standard since the high frequency components generated by the modulation process are not properly attenuated when off-nominal frequencies are present. On the contrary, the proposed model satisfies the accuracy limits for phasor, frequency and ROCOF estimation for both P class and M class.

4) OOB Interference Test

The OOB interference test assesses the immunity to interharmonic pollution. It is the most important issue for M class, and is the most challenging test. For this test, synthetic sinusoidal signals at 57, 60 and 63 Hz with several values of OOB interference have to be tested. The OOB interference corresponds to sinusoidal signals at 10% of the magnitude of the fundamental component, ranging from 10 to 120 Hz but omitting the range within the Nyquist frequency $\pm fps/2$ around the fundamental frequency where *fps* stands for the number of frames per second. As shown in Fig. 4(e), both algorithms have admissible accuracy levels for phasor estimation. However, out-of-range values are obtained by the reference model for frequency estimation close to the Nyquist frequency boundaries (30 Hz and 90 Hz) when the frequency deviation is present. A maximum FE value of 0.0114 Hz is also obtained over the allowable FE (0.01 Hz) as shown in Table I. On the contrary, the FE value for the proposed algorithm is 0.0073 Hz within the accuracy requirements. Regarding the TVE values, both algorithms accomplish the accuracy requirements with 0.037% and 0.046% for the reference model and the proposed algorithm, respectively.

5) Total Harmonic Test

The harmonic rejection test is carried out through the analysis of synthetic signals that contain total harmonic distortion (THD) values of 1% for P class and 10% for M class. In these signals, each harmonic up to the 50th is considered. As depicted in Fig. 4(f), both algorithms have the required accuracy for P class and M class, where lower error levels are achieved by the proposed algorithm for M class. In Table I, the maximum errors are summarized where the TVE values of 7.93×10^{-6} for M class in the reference model algorithm and 1.01×10^{-6} for the proposed algorithm are observed. Likewise, the FE and RFE values accomplish the accuracy requirements with maximum values of 1.53×10^{-12} Hz and 1.07×10^{-10} Hz/s obtained by the reference model and 0.003 Hz and 2.67×10^{-8} Hz/s for the proposed model, respectively.

TABLE I
MAXIMUM ERROR VALUES FOR STEADY-STATE TESTS

Test	Class	Standard reference algorithm			Proposed algorithm		
		TVE	FE (Hz)	RFE (Hz/s)	TVE	FE (Hz)	RFE (Hz/s)
Voltage magnitude	P	2.34×10^{-14}			1.57×10^{-8}		
	M	7.69×10^{-6}			9.93×10^{-10}		
Current magnitude	P	2.34×10^{-14}			1.57×10^{-8}		
	M	7.69×10^{-6}			9.93×10^{-10}		
Frequency	P	4.09×10^{-4}	3.31×10^{-2}	8.291×10^{-1}	4.42×10^{-6}	2.27×10^{-4}	5.70×10^{-3}
	M	1.05×10^{-5}	1.10×10^{-3}	6.510×10^{-2}	2.60×10^{-5}	4.67×10^{-4}	1.85×10^{-2}
Phase	P	4.60×10^{-6}			1.05×10^{-6}		
	M	8.49×10^{-6}			2.57×10^{-6}		
OOB interference	P	3.71×10^{-4}	1.14×10^{-2}		4.60×10^{-4}	7.30×10^{-3}	
THD	P	6.76×10^{-14}	1.53×10^{-12}	1.070×10^{-10}	5.00×10^{-5}	3.00×10^{-3}	2.67×10^{-8}
	M	7.93×10^{-6}	8.71×10^{-4}		1.01×10^{-6}	2.47×10^{-5}	

B. Dynamic Test

1) Amplitude Modulation Test

The modulation test is performed according to the standard [4]. In this case, the modulation test is carried out using a frequency change from 58 to 62 Hz in steps of 0.2 Hz for P class and 55-65 Hz in steps of 0.2 Hz for the M class. Regarding the obtained results, the error values for the reference model and the proposed algorithm are below the limits stated in the standard as shown in Fig. 5(a). In this figure, the amplitude modulation test for P class and M class is depicted as well as their respective TVE, FE, and RFE values. The blue line represents the maximum values for the standard algorithm and the orange line represents the values for the proposed algorithm. In Table II, it can be seen that both algorithms are below the limits, e.g., the maximum TVE value for the proposed algorithm is 0.0316% whereas the algorithm defined by the standard obtains a TVE value of 0.0375%, which indicates that the proposed algorithm estimates a more accurate result. On the other hand, for the M class, only the TVE value is greater than the values obtained from the algorithm for the standard. However, these values are within the limits stablished [4], [5].

2) Phase Modulation Test

For this test, a modulation in phase is carried out according to the characteristics specified in the standard [4]. Figure 5(b) shows the maximum values obtained by the reference and the proposed algorithms. In these graphs, it can be seen that for the M class, the TVE, FE, and RFE values for the reference algorithm are lower than those obtained by the proposed algorithm. On the other hand, the TVE and RFE values of the algorithm proposed for P class are lower than the reference algorithm. Nevertheless, both methodologies are within the limits defined by the standard. For example, the RFE value for P class obtained by the reference algorithm is 0.0185, whereas the value for the proposal is 0.0175; yet, both values are below the limit defined by the standard. In Table II, the maximum values are concentrated.

3) Positive and Negative Ramp Tests

In Fig. 5(c) and (d), the positive and negative ramp tests as well as the values for TVE, FE, and RFE are shown, respectively, where the values of the proposed algorithm are below the values of the standard algorithm for the P class. Regarding the M class, a change in the TVE value can be denoted, where the value for the standard is lower than the one of the proposed methodologies, but a smoother behavior is observed for the proposed algorithm. Both algorithms provide results that fall within the limits presented in the standard, including FE and RFE. For instance, for the positive ramp test, the values of TVE, FE, and RFE for the proposed algorithm are 0.0114%, 6.03×10^{-4} Hz and 0.0014 Hz/s, respectively. On the contrary, the values obtained by the reference algorithm are 0.0345%, 0.0209 Hz, and 0.4768 Hz/s, respectively. These results indicate that the proposed algorithm can handle the deviation frequency in a better way than the reference algorithm. It should be noticed that the behaviors are similar in both ramp tests. In Table II, the maximum values of each test are concentrated. For these values, the obtained results during the transition time (two sample periods before and after a change in the test ROCOF) in Fig. 5(c) and (d) are discarded [4].

4) Step Test

The time performance evaluation is carried out using step changes in phase and magnitude. The step test uses the transition between two states to establish the response and delay time as well as the overshoot in the measurements. In this regard, a set of shifted steps by a constant fraction of the reporting interval are used [4]. It is important to mention that the response and delay time is small compared to the PMU reporting time. Thus, the results for each step can be interleaved in order to have a response curve with a higher resolution [4], [27]. The delay time corresponds to the time when the stepped parameter achieves a value of 50% (horizontal line) between the starting and ending steady-state values shown in Fig. 6(a). On the other hand, the response time is defined as the difference between the time in which the signal leaves a specified accuracy limit and the time in which it returns and remains within this limit. Hence, the response time is determined from the error measurements of TVE, FE, and RFE. Figure 6(b) and (c) shows an example to present how the values of the proposed algorithm are obtained. For instance, the step change in magnitude test for M class is shown in Fig. 6(b), where the red line is the limit for the delay time proposed by the standard and the green square is the area where the 50% of the value is achieved between the starting and ending steady states, as seen in the zoomed area. Table III shows a comparison about delay time, response time, and overshoot values for both algorithms. The value for delay time of the proposed algorithm is 9.65×10^{-5} and that of the standard is 9.97×10^{-5} for P class, where both values are lower than the maximum value defined by the standard [4]. In Fig. 6(c), it can be observed the general process to calculate the response time. The first picture shows the zone for the difference between the time in which the signal leaves and returns within the limit (represented by the green square). The second picture presents the zoomed area denoted by the green square, where it can be seen the zone for the response time associated to the step change in magnitude test for M class. From Table III, it is seen that the value for the proposed methodology is 0.049 s and the value for the algorithm presented by the standard is 0.033 s. Although the values of the proposal are slightly higher in some cases, all the values shown in Table III are below the limit values in the standard.

C. Comparison with Previous Works

Based exclusively on previous works with the methods focused on satisfying both P class and M class requirements [4], [16]-[19], the proposed method presents some important features that have to be highlighted. Unlike the proposed method which presents a unique filter design method for both classes of PMU by changing the filter order only, different strategies have been used in other works: ① a symmetric triangular filter for P class and a sinc filter for M class [4]; ② an asymmetric algorithm for P class and the Tick-Tock algorithm for M class [18]. In [16], [19], a unique method is also used as basis for both PMU classes, i.e., the

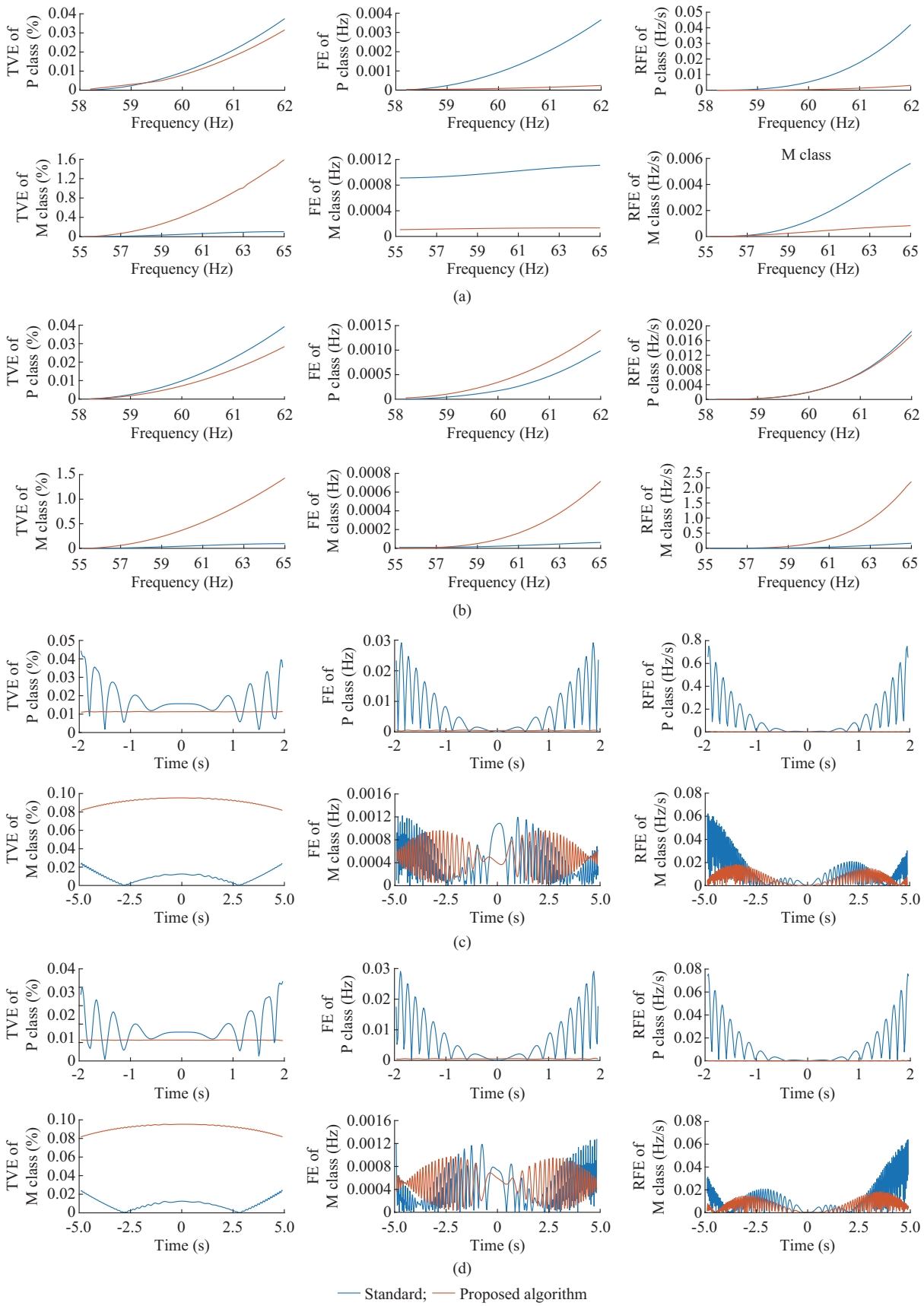

Fig. 5. Dynamic tests for PMUs: P class and M class. (a) Magnitude modulation test. (b) Phase modulation test. (c) Positive ramp test. (d) Negative ramp test.

TABLE II
MAXIMUM ERROR VALUES FOR DYNAMIC TESTS

Test	Class	Standard reference algorithm			Proposed algorithm		
		TVE (%)	FE (Hz)	RFE (Hz/s)	TVE (%)	FE (Hz)	RFE (Hz/s)
Amplitude modulation	P	0.0375	0.003700	0.0421	0.0316	0.000237	0.003100
	M	0.1043	0.001100	0.0056	1.5892	0.000133	0.000843
Phase modulation	P	0.0392	0.000986	0.0185	0.0284	0.001400	0.017500
	M	0.0956	0.006200	0.1647	1.4303	0.071600	2.204800
Positive ramp	P	0.0345	0.020900	0.4768	0.0114	0.000603	0.001400
	M	0.0216	0.001200	0.0597	0.0953	0.000964	0.018500
Negative ramp	P	0.0343	0.020800	0.4639	0.0114	0.000605	0.001400
	M	0.0216	0.001300	0.0589	0.0953	0.000973	0.018400

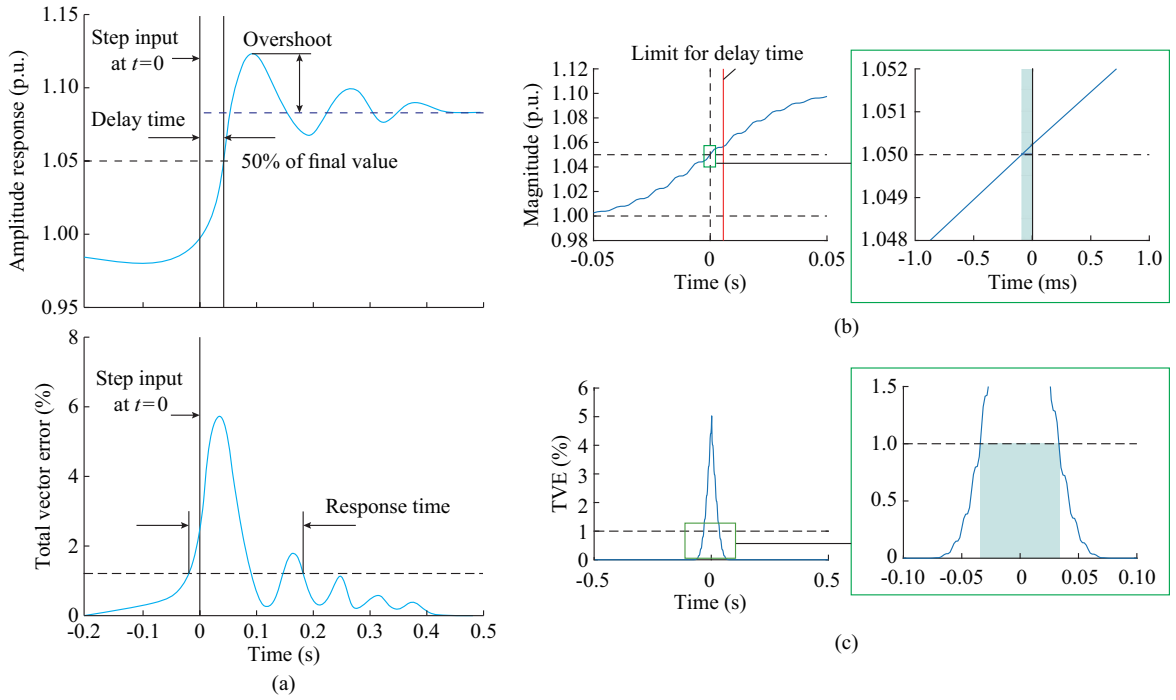

Fig. 6. Step change test. (a) Reference for step change test. (b) Example test for delay time. (c) Example test for response time.

TABLE III
STEP CHANGE RESULTS

Test	Algorithm	Delay time (s)	Response time (s)	Frequency response time (s)	ROCOF response (s)	Over-shoot (s)
P-step magnitude	Reference	9.97×10^{-5}	0.033	0.033	0.0497	0
	Proposed	9.65×10^{-5}	0.027	0.032	0.0480	0
P-step phase	Reference	8.27×10^{-4}	0.025	0.033	0.0500	0
	Proposed	7.63×10^{-4}	0.021	0.032	0.0480	0
M-step magnitude	Reference	9.33×10^{-5}	0.033	0.087	0.1400	6.0
	Proposed	9.58×10^{-5}	0.049	0.084	0.1200	0
M-step phase	Reference	7.60×10^{-4}	0.070	0.151	0.1750	5.9
	Proposed	7.55×10^{-4}	0.058	0.129	0.1590	0

GTWLS-IpDFT [16] and the TFT [19]. However, additional stages are required such as the proper selection of the number of waveform cycles, the extraction of most significant disturbances, and a detector of signals in steady state or with fast changes. Regarding the OOB test, one of the most difficult and demanding tests, the proposed algorithm has achieved satisfactory results due to the proposed filter design methodology. On the contrary, the fulfilment of the OOB test is still an unsolved issue [18].

On the other hand, it should be pointed out that other

works in the literature have presented some specialized and sophisticated methods for a specific PMU class, i.e., P class or M class, where very promising results have been obtained in terms of speed, harmonic and interharmonic rejection, tracking capabilities, etc. However, the goal of this paper is not to provide a method that outperforms the capabilities of a specialized algorithm in one class, but to provide a unique method that allows satisfying the requirements stated by the standard for both classes, simplifying the PMU setup in different applications of modern power systems that could require P class or M class capabilities. Also, some features that are supposed to be for a specific PMU class are exploited in both classes since the same filter design methodology is used in the proposal. Finally, the proposed algorithm represents a low-complex and low-computational-burden solution since it only requires the application of the designed FIR filter during an online and continuous phasor estimation.

V. Conclusion

In this paper, new phasor estimators based on complex brick-wall band-pass filters that satisfy the requirements of the phasor estimators in P class and M class PMUs are presented. The WLS method is used to obtain the complex filter by means of a weighting function proposed to improve the fit in the passband and the rejection in the valleys. In the weighting function, the weights based on Gaussian functions allow having a good rejection to harmonic content at the stop band, which is important to satisfy the tests related to harmonic content. The complex filters are integrated into a PMU scheme by estimating phasor, frequency, and ROCOF parameters to validate their performance by means of all the benchmark tests recommended in the IEEE Std. C37.118.1-2011 along with its amendment in the IEEE Std. C37.118.1a-2014, where a comparative analysis with the reference algorithm of the standard is carried out.

All tests are evaluated using a reporting rate of 60 fps which is one of the most demanding conditions for 60 Hz systems. Requirements for TVE, FE, RFE, overshoot, response time, and delay time are presented, where none of the maximum limits established by the standard are exceeded by the proposed algorithm, demonstrating the usefulness and effectiveness of the proposed algorithm. On the contrary, inconveniences are come up in the reference model algorithm in the frequency and OOB interference tests, especially for FE and RFE values. Unlike other works, the same methodology is successfully used for both classes of PMUs, where the filter order is the only parameter that changes. This is expected since the error requirements for both classes are quite different. It is important to mention that once the filters are designed, no further processing stages are required unlike other works that implement different algorithms, including the reference model presented by the standard which requires a modulation process. These stages increase the computational burden. Therefore, the main advantage of the proposed phasor estimator is the low complexity (FIR filter) and features of rejection to harmonic and interharmonic content, where the benefits provided by the proposed design can be applied to both classes.

References

[1] F. Aminifar, M. Fotuhi-Firuzabad, A. Safdarian *et al*., "Synchrophasor measurement technology in power systems: panorama and state-of-the-art," *IEEE Access*, vol. 2, pp. 1607-1628, Dec. 2014.

[2] A. Ikbal, M. A. Aftab, and S. S. Hussain, "Performance comparison of IEC 61850-90-5 and IEEE C37.118.2 based wide area PMU communication networks," *Journal of Modern Power Systems and Clean Energy*, vol. 4, no. 3, pp. 487-495, Jul. 2016.

[3] A. G. Phadke and T. Bi, "Phasor measurement units, WAMS, and their applications in protection and control of power systems," *Journal of Modern Power Systems and Clean Energy*, vol. 6, no. 4, pp. 619-629, Jul. 2018.

[4] Standard for synchrophasor measurements for power systems, IEEE C37.118.1-2011, 2011.

[5] Standard for synchrophasor measurements for power systems-Amendment 1: modification of selected performance requirements, IEEE C37.118.1a-2014, 2014.

[6] F. Messina, P. Marchi, L. R. Vega *et al*., "A novel modular positive-sequence synchrophasor estimation algorithm for PMUs," *IEEE Transactions on Instrumentation & Measurement*, vol. 66, no. 6, pp. 1164-1175, Dec. 2016.

[7] J. R. Razo-Hernandez, M. Valtierra-Rodriguez, D. Granados-Lieberman *et al*., "A phasor estimation algorithm based on Hilbert transform for P-class PMUs," *Advances in Electrical and Computer Engineering*, vol. 18, no. 3, pp. 97-104, Aug. 2018.

[8] P. Tosato, D. Macii, M. Luiso *et al*., "A tuned lightweight estimation algorithm for low-cost phasor measurement units," *IEEE Transactions on Instrumentation & Measurement*, vol. 67, no. 5, pp. 1047-1057, Jan. 2018.

[9] D. Belega, D. Macii, and D. Petri, "Fast synchrophasor estimation by means of frequency-domain and time-domain algorithms," *IEEE Transactions on Instrumentation & Measurement*, vol. 63, no. 2, pp. 388-401, Feb. 2014.

[10] C. Guido, A. Vaccaro, and D. Villacci, "A review of the enabling methodologies for PMUs-based dynamic thermal rating of power transmission lines," *Electric Power Systems Research*, vol. 152, pp. 257-270, Nov. 2017.

[11] S. Affijulla and P. Tripathy, "Development of phasor estimation algorithm for P-class PMU suitable in protection applications," *IEEE Transactions on Smart Grid*, vol. 9, no. 2, pp. 1250-1260, Mar. 2018.

[12] A. J. Roscoe, B. Dickerson, and K. E. Martin, "Filter design masks for C37.118.1 a-compliant frequency-tracking and fixed-filter M-class phasor measurement units," *IEEE Transactions on Instrumentation & Measurement*, vol. 64, no. 8, pp. 2096-2107, Aug. 2015.

[13] A. Abdolkhalig and R. Zivanovic, "Phasor measurement based on IEC 61850-9-2 and Kalman-filtering," *Measurement*, vol. 50, pp. 126-134, Apr. 2014.

[14] T. Bi, H. Liu, Q. Feng *et al*., "Dynamic phasor model-based synchrophasor estimation algorithm for M-class PMU," *IEEE Transactions on Power Delivery*, vol. 30, no. 3, pp. 1162-1171, Jun. 2015.

[15] A. Shaik and P. Tripathy, "Development of phasor estimation algorithm for P-class PMU suitable in protection applications," *IEEE Transactions on Smart Grid*, vol. 9, no. 2, pp. 1250-1260, Mar. 2018.

[16] D. Belega, D. Fontanelli, and D. Petri, "Dynamic phasor and frequency measurements by an improved Taylor weighted least squares algorithm," *IEEE Transactions on Instrumentation & Measurement*, vol. 64, no. 8, pp. 2165-2178, Aug. 2015.

[17] A. Derviškadić, P. Romano, and M. Paolone, "Iterative-interpolated DFT for synchrophasor estimation: A single algorithm for P- and M-class compliant PMUs," *IEEE Transactions on Instrumentation & Measurement*, vol. 67, no. 3, pp. 547-558, Mar. 2018.

[18] A. J. Roscoe, F. Abdulhadi, and G. M. Burt, "P and M class phasor measurement unit algorithms using adaptive cascaded filters," *IEEE Transactions on Power Delivery*, vol. 28, no. 3, pp. 1447-1459, Jul. 2013.

[19] P. Castello, J. Liu, C. Muscas *et al*., "A fast and accurate PMU algorithm for P+M class measurement of synchrophasor and frequency," *IEEE Transactions on Instrumentation & Measurement*, vol. 63, no. 12, pp. 2837-2845, Dec. 2014.

[20] P. Castello, M. Lixia, C. Muscas *et al*., "Impact of the model on the accuracy of synchrophasor measurement," *IEEE Transactions on Instrumentation & Measurement*, vol. 61, no. 8, pp. 2179-2188, Aug. 2012.

[21] T. Miyata, K. Teramoto, and N. Aikawa, "A design method for FIR filters with complex coefficients by successive projection method," in *Proceedings of IEEE International Symposium on Information Theory*

and its Applications, Honolulu, USA, Oct. 2012, pp. 275-278.
[22] A. Mejia-Barron, D. Granados-Lieberman, J. R. Razo-Hernandez *et al*., "Harmonic PMU algorithm based on complex filters and instantaneous single-sideband modulation," *Electronics*, vol. 8, no. 2, pp. 135, Jan. 2019.
[23] Y. L. Shen, Y. Q. Tu, L. J. Chen *et al*., "Phase difference estimation method based on data extension and Hilbert transform," *Measurement Science & Technology*, vol. 26. no. 9, Jul. 2015.
[24] S. L. Marple, "Computing the discrete-time analytic signal via FFT," *IEEE Transactions on Signal Processing*, vol. 47, no. 9, pp. 2600-2603, Sept. 1999.
[25] M. Owen, "Practical signal processing," Cambridge, UK: Cambridge University Press, 2007.
[26] J. H. Lee, C. K. Chen, and Y. C. Lim, "Design of discrete coefficient FIR digital filters with arbitrary amplitude and phase responses," *IEEE Transactions on Circuits and Systems II: Analog and Digital Signal Processing*, vol. 40, no. 7, pp. 444-448, Jul. 1993.
[27] K. E. Martin, "Synchrophasor measurements under the IEEE standard C37.118.1-2011 with amendment C37.118.1a," *IEEE Transactions on Power Delivery*, vol. 30, no. 3, pp. 1514-1522, Jun. 2015.

Jose R. Razo-Hernandez received the B.E. degree in Electronics Engineering and the M.E. degree in Electrical Engineering from the University of Guanajuato, Guanajuato, Mexico, in 2006 and 2009, respectively, and the Ph.D. degree in Mechatronics from the Autonomous University of Queretaro, San Juan del Rio, Mexico, in 2019. He is currently a professor with the Higher Technological Institute of Irapuato, Guanajuato, Mexico. His research interests include PMUs, power quality, expert systems, hardware signal processing and mechatronics.

Arturo Mejia-Barron received the B.S., M.S., and Ph.D. degrees in Mechatronics from Autonomous University of Queretaro, Queretaro, Mexico, in 2013, 2015 and 2019, respectively. His research interests include power electronics, signal processing and electrical systems.

David Granados-Lieberman received the B.S. and M.S. degrees in Electrical Engineering from Universidad de Guanajuato, Guanajuato, Mexico, in 2007 and 2009, respectively. He received the Ph.D. degree in Electrical Engineering from the Autonomous University of Queretaro, Queretaro, Mexico, in 2013. He is currently a professor in the bachelor's program of electromechanical engineering and master program of electrical engineering at the Higher Technological Institute of Irapuato, Guanajuato, Mexico. His research interests include monitoring and diagnostics of electrical machines, power quality, and applications of digital signal processing.

Martin Valtierra-Rodriguez received the B.E. degree in Mechatronics Engineering and the M.E. degree in Electrical Engineering from the University of Guanajuato, Guanajuato, Mexico, in 2008, and 2010, respectively, and the Ph.D. degree in Mechatronics from the Autonomous University of Queretaro, San Juan del Rio, Mexico, in 2013. He is currently a professor with the Faculty of Engineering, Autonomous University of Queretaro, San Juan del Rio, Mexico. He is the IEEE Senior Member, 2018, and a member of the Mexican National Research System. His current research interests include power quality, fault diagnostics, expert systems, and signal processing.

Jose F. Gomez-Aguilar received the B.S. and M.Eng. degrees in Electrical Engineering from the University of Guanajuato, Guanajuato, Mexico, in 2005 and 2007, respectively, and Ph.D. degree in Physical from DCI-Campus León, University of Guanajuato, Guanajuato, Mexico, in 2012. He is currently a full research professor at the Electronics Engineering Department of the National Research and Technological Development Center (CENIDET), Cuernavaca, Mexico. His research interests include image and signal processing, control, power quality analysis.